IEEE Access
Multidisciplinary ⋮ Rapid Review ⋮ Open Access Journal

Received May 11, 2022, accepted May 26, 2022, date of publication June 8, 2022, date of current version June 23, 2022.

Digital Object Identifier 10.1109/ACCESS.2022.3180731

Calculation Method for Dynamic Stiffness of Multispan Overhead Transmission Lines

LV ZHONGBIN[1,2], ZHANG BO[2], LIU XIAOHUI[3], TAO YAGUANG[2], LIANG HAOBO[4], LI QING[2], AND YAN BO[1]

[1]College of Aerospace Engineering, Chongqing University, Chongqing 400044, China
[2]State Grid Henan Electric Power Research Institute, Zhengzhou 450052, China
[3]State Key Laboratory of Mountain Bridge and Tunnel Engineering, Chongqing Jiaotong University, Chongqing 400074, China
[4]School of Civil Engineering, Chongqing Jiaotong University, Chongqing 400074, China

Corresponding author: Liu Xiaohui (cqdxlxh@126.com)

This work was supported in part by the Research Project of the State Grid Corporation of China under Grant 5200-202024142A-0-0-00.

ABSTRACT The dynamic motion of a span is coupled to the other spans in transmission lines. From the continuity conditions, force equilibrium conditions, and dynamical equations of every span conductor and insulator string, a close-form expression for the dynamic stiffness of a coupled two spans in harmonic motion is presented. Unlike some existing theories of single span conductor, the effect between the conductors and insulator strings is considered here. By means of example calculations, the validity of the dynamic stiffness of two-span is demonstrated by the consistency of the results determined by the ABAQUS. Meanwhile, the dynamic stiffness and natural frequency are discussed under variation of the span lengths ratio, Irvine parameter, and insulator string length. Moreover, the modal shape function corresponding natural frequency is derived, and the contribution of localization mode is studied. The results show that the contribution is either sensitive to or independent of transmission line parameters in certain parameter ranges. Finally, generalizing the work of two-span, the dynamic stiffness of arbitrary span number is obtained.

INDEX TERMS Equivalent stiffness, series of spans, mode, natural frequency, ABAQUS.

I. INTRODUCTION

Using insulator string to connect a span with its adjacent span and forming multi-span structure are widely used in electricity transmission lines. Galloping is a well-known phenomenon for iced electricity transmission lines. Galloping of multi-span conductors can reach high amplitude causing high tension on conductors, and the periodic change of the tension can be leaded to damage of sub-conductors, spacers, and towers (Kermani *et al.*, 2013; Chen *et al.*, 2017), which usually give rise to disruption of power supply, as shown in Fig.1. In January 2018, a serious cold snap swept through much of northern and central china, knocking down the regional power lines due to galloping [3].

For the analysis of the galloping and other dynamic response of transmission lines, the first basic and most important aspect is to obtain vibratory characteristic of transmission lines as low-sag cables. Initially, the linear theory of free vibration of single-span horizontal cable with small sag was studied by Irvine (1974). Meanwhile, an important geometric-elastic parameter λ was raised, and the natural frequencies and corresponding symmetrical in-plane modes depended on the parameter. Irvine (1978) generalized the theory of horizontal cable and applied it to an inclined cable. Yamaguchi (1979) considered the weight component parallel to the chord of an inclined cable and studied natural frequencies and modal shapes of the inclined cable.

(a) Damage of the tower arm; (b)Damage of the spacer

FIGURE 1. Overhead transmission lines.

The associate editor coordinating the review of this manuscript and approving it for publication was Diego Bellan.

Triantafyllou (1984, 1986) found that for inclined cable an ''avoided crossing'' on frequency curves occurs. Afterward, in order to avoid complicated calculation, Wu *et al.* (2005) and Zhou *et al.* (2011) presented a simplified method by using two characteristic parameters λ and ε. In order to study the dynamic response of cable-tower, cable-bridge, and other cable-supported structures, Veletsos *et al.* (1983) proposed the dynamic stiffness of single span cable. The dynamic stiffness can evaluate the deformation resistance (Kim *et al.*, 2001; Han *et al.*, 2017), and can identify the frequencies of corresponding deferent modes (Li *et al.*, 2017; Dai *et al.*, 2017; Kari *et al.*, 2017). Because the cable is a flexible structure, the cable exhibits very rich nonlinear dynamic response. In particular, if two or more linear natural frequencies are nearly commensurable, these commensurable relationships of frequencies can cause the multiple modes to be strongly coupled, and an internal resonance occurs (Rega *et al.*, 1999, 2004).

Most of the interesting internal resonances occur at the crossover points in the spectrum of cable natural frequencies. Based on the obtained modes and corresponding frequencies, a multimode discretization of the continuum formulations is adopted, then a simplified asymptotic analysis is applied by using any perturbation technique (Lacarbonara *et al.*, 2003; Srinil *et al.*, 2007). In recent decades, a lot of results, which include internal resonance and multiple internal resonances (Abe *et al.*, 2010; Zhao *et al.*, 2006; Wang *et al.*, 2009), are obtained for single span cable nonlinear vibrations. Luogno *et al.* (1998, 2008, 2009) discovered that the internal resonance can occur in transmission line galloping, and further investigated the nonlinear galloping instability of single span under multiple internal resonance conditions. Afterward, using finite element method, liu *et al.* (2009) also discovered the internal resonance through the study of iced quad-bundle conductor galloping.

Nonlinear dynamic characteristics of self-excited vibration for iced transmission line have been recently studied (Liu *et al.*, 2010; Yan *et al.*, 2012; Liu *et al.*, 2015; Guo *et al.*, 2017). However, the nonlinear dynamic investigations are only based on single span transmission lines (Lou *et al.*, 2014; Ghabraei *et al.* 2016; Zhang *et al.*, 2017; Nguyen *et al.*, 2018). In overhead transmission lines, the bare wire conductors are suspended from towers via insulator strings. Overhead transmission lines between two anchoring towers, which is connected to tangent towers in a row by a freely movable insulator string, is called a strain section. Due to the swing of suspension insulator strings along a transmission line, it is possible for coupling to occur between different spans in a strain section (Rienstra, 2005). Initially, in order to simplify the calculation, a single-span model with spring boundary conditions, in which suspension insulator string and adjacent span are represented by equivalent linear spring, is established (Yu *et al.*, 1993; Desai *et al.*, 1995; Guo *et al.*, 2018). Afterward, the effect of the spring boundary conditions on galloping amplitude is compared to the effect of the previous fixed boundary conditions by using

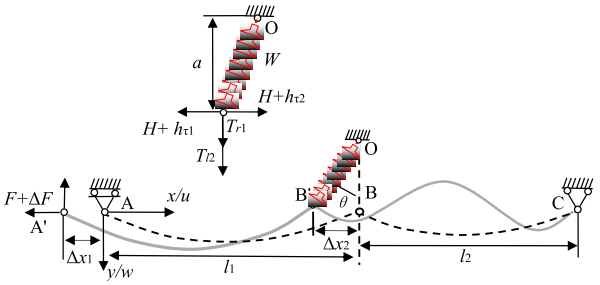

FIGURE 2. The dynamic stiffness of two-span transmission line with insulator string.

FEM (Wang *et al.*, 2009, 2010). The results showed that the boundary conditions of a single span can significantly influence the galloping amplitude. The dynamic interaction between the adjacent spans is reflected in the equivalent stiffness spring at both ends of single span. In fact, the equivalent stiffness represented adjacent spans not only depends on the cable geometrical parameters, but also depends on the frequency of external excitation. In addition, in order to understand the interaction between the multiple spans, Xie *et al.* (2017) studied the effect of the span ratio on the frequencies of two-span transmission lines, and Yi *et al.* (2017) studied the vibratory characteristics of a three-span mass-carrying cable with multiple pulley supports.

Further investigation on the interaction between different spans in a strain section is important to deeply understand the nonlinear galloping characteristics of transmission lines, such as multi-span internal resonance conditions, frequency, mode of multi-span vibration, and the effect of the multi-span conductors on the towers. This paper is intended to be responsive to these needs. Since the two-span transmission lines is a simplest multi-span transmission lines, we introduce a dynamic stiffness model of two-span transmission lines that right end is fixed and the left end is subjected to a harmonically varying horizontal displacement. The configuration of every span conductor is considered to have a parabolic profile at static equilibrium position under self-weight, the displacement at the left end is presumed to be small. The effect of span ratio, insulator string length, and external exciting frequency on the dynamic stiffness is discussed, respectively. Special attention is paid to the identification of frequencies through dynamic stiffness peaks. The accuracy of obtained frequencies and corresponding modes is discussed through comparison of theoretical and FEM results. Finally, the two-span dynamic stiffness is generalized to the case of arbitrary multi-span transmission lines. The results can provide a theoretic foundation for the development of the galloping research.

II. DYNAMIC STIFFNESS FOR TWO-SPAN CONDUCTOR

A. THEORETICAL FORMULA TO CALCULATE THE DYNAMIC STIFFNESS

A transmission line suspended from end supports located at equal elevation is considered, as shown in Fig.2. The support A is a smooth roller, and the support C is a hinge. The support

B is moving in concentric circles with centers at O because the transmission line hangs from the insulator string OB. The dotted line represents the static equilibrium configuration under self-weight. The transmission line is linearly elastic, with negligible bending stiffness, uniform undeformed effective cross-section A, self-weight per unit length p, and Young's modulus E. l_1 and l_2 are span length, which is the horizontal length of the straight line between two supports in a span. The transmission line is also called flexible cable because the span length of a transmission line is much greater than the dimension. For the selected Cartesian coordinate system, the x-direction takes along the cable chord, the y-direction takes the normal direction, and the origin is taken at the left end of a span. The static equilibrium configuration of small sag horizontal cable is defined by the parabola

$$y = \frac{ql^2}{2H}\left(\frac{x}{l} - \left(\frac{x}{l}\right)^2\right) \tag{1}$$

where l is the horizontal span. The H is the horizontal component of cable tension which is constant everywhere. If the left end A of the cable is subjected to an additional harmonically varying horizontal force $\Delta F = \Delta\bar{F}e^{i\omega t}$, the dynamic configuration of the cable is the solid line as shown in Fig.2. The transmission line dynamics is described by the horizontal u and vertical w displacement components measured from the static configuration. The amplitude of additional force ΔF is presumed to be small, so that the displacement of the left end is also small. The vibration of two-span cable with respect to its position of static equilibrium can be expressed by the partial differential equations [3]

$$H\frac{\partial^2 w_1}{\partial x^2} + \Delta F\frac{\mathrm{d}^2 y_1}{\mathrm{d}x^2} = m\frac{\partial^2 w_1}{\partial t^2} + c\frac{\partial w_1}{\partial t} \tag{2a}$$

$$H\frac{\partial^2 w_2}{\partial x^2} + h_{\tau 2}\frac{\mathrm{d}^2 y_2}{\mathrm{d}x^2} = m\frac{\partial^2 w_2}{\partial t^2} + c\frac{\partial w_2}{\partial t} \tag{2b}$$

where m is mass per unit length; c is the coefficient of viscous damping per unit of chord length; $\Delta h_{\tau 2}$ is the dynamic additional tension of H. The effects of the axial components of the inertia forces on the dynamic stiffness are small compared with those of the y-direction components, and may be neglected. The ΔF is equal to $\Delta h_{\tau 1}$ when the axial inertia force of a cable is neglected. By substituting (1) into (2), the (2) can be simplified, as

$$H\frac{\partial^2 w_1}{\partial x^2} - m\frac{\partial^2 w_1}{\partial t^2} - c\frac{\partial w_1}{\partial t} = \frac{q\Delta F}{H} \tag{3a}$$

$$H\frac{\partial^2 w_2}{\partial x^2} - m\frac{\partial^2 w_2}{\partial t^2} - c\frac{\partial w_2}{\partial t} = h_{\tau 2}\frac{q}{H} \tag{3b}$$

The insulator string shown in Fig.1 is suspended from a smooth bearing at O. The insulator string which oscillates with a small amplitude executes harmonic motion. The insulator string has an angular displacement of θ measured from the equilibrium position at the instant. The sun of the moments about O of all the external forces is equal to $J\ddot{\theta}$, the moment of inertia J with the weight W relative to O is $\frac{W}{3g}a$ and $\ddot{\theta}$ is the angular acceleration. Thus,

$$a(h_{\tau 1} - h_{\tau 2}) - (T_{r1} + T_{l2})\Delta x_2 - W\frac{\Delta x_2}{2} = J\ddot{\theta} \tag{4}$$

were a is the length of the insulator string, Δx_2 is the displacement of the lower end B. T_{r1} and T_{l2} are vertical forces exerted by the two-span conductors at the lower end B.

In conditions of moderately small vibration amplitudes and assuming small sag, the additional tension becomes [3]

$$h_\tau\left(\frac{\mathrm{d}x}{\mathrm{d}s}\right)^3 = EA\left(\frac{\partial u}{\partial x} + \frac{\mathrm{d}y}{\mathrm{d}x}\frac{\partial w}{\partial x}\right) \tag{5}$$

Accounting for the cable boundary conditions and compatibility of the resulting strains and displacements, the additional tensions of two-span conductors are given

$$h_{\tau 1} = \Delta F = \frac{EA}{L_{e1}}\left[(\Delta x_1 - \Delta x_2) + \frac{q}{H}\int_0^{l_1} w_1(x,t)dx\right] \tag{6a}$$

$$h_{\tau 2} = \frac{EA}{L_{e2}}\left[\Delta x_2 + \frac{q}{H}\int_0^{l_2} w_2(x,t)\mathrm{d}x\right] \tag{6b}$$

$L_{\mathrm{e}1}$ and $L_{\mathrm{e}1}$ are the effective lengths of two-span conductors.

For harmonically excited two-span conductors, the values of the displacement increment and additional tension are of the form:

$$\Delta F = \Delta\bar{F}e^{i\omega t};\quad h_{\tau 1} = \bar{h}_{\tau 1}e^{i\omega t};\quad h_{\tau 2} = \bar{h}_{\tau 2}e^{i\omega t} \tag{7a}$$

$$w_1(x,t) = \bar{w}_1(t)e^{i\omega t};\quad w_2(x,t) = \bar{w}_2(t)e^{i\omega t} \tag{7b}$$

$$\Delta x_1 = \Delta\bar{x}_1 e^{i\omega t};\quad \Delta x_2 = \Delta\bar{x}_2 e^{i\omega t} \tag{7c}$$

Apply (7), the system equations (3) can be written as:

$$H\frac{\mathrm{d}^2\bar{w}_1}{\mathrm{d}x^2} + (m\omega^2 - i\omega c)\bar{w}_1 = \frac{q\bar{h}_{\tau 1}}{H} \tag{8a}$$

$$H\frac{\mathrm{d}^2\bar{w}_2}{\mathrm{d}x^2} + (m\omega^2 - i\omega c)\bar{w}_2 = \frac{q\bar{h}_{\tau 2}}{H} \tag{8b}$$

When the angular displacement of θ is small, the θ is equal approximately to $\Delta x_2/a$. With this approximation and (7) the (4) lead to the following expression as

$$a(\bar{h}_{\tau 1} - \bar{h}_{\tau 2}) - \left(T_{r1} + T_{l2} + \frac{W}{2} - \frac{J\omega^2}{a}\right)\Delta\bar{x}_2 = 0;\qquad \bar{h}_{\tau 1} = \Delta\bar{F} \tag{9}$$

The solution of (8), with the given boundary conditions, is

$$\bar{w}_1(x) = \left(\frac{l_1}{\bar{\omega}_1 H}\right)^2 q h_{\tau_1}\left(1 - \tan\left(\frac{\bar{\omega}_1}{2}\right)\sin\left(\bar{\omega}_1\frac{x}{l_1}\right) - \cos\left(\bar{\omega}_1\frac{x}{l_1}\right)\right) \tag{10a}$$

$$\bar{w}_2(x) = \left(\frac{l_2}{\bar{\omega}_2 H}\right)^2 q h_{\tau_2}\left(1 - \tan\left(\frac{\bar{\omega}_2}{2}\right)\sin\left(\bar{\omega}_2\frac{x}{l_2}\right) - \cos\left(\bar{\omega}_2\frac{x}{l_2}\right)\right) \tag{10b}$$

where $\bar{\omega}_1^2 = (m\omega^2 - \omega ci)l_1^2/H$, $\bar{\omega}_2^2 = (m\omega^2 - \omega ci)l_2^2/H$. The additional tensions, $h_{\tau 1}$ and $h_{\tau 2}$, may now be evaluated from (6). Substituting the (10) into the (6), the following expressions of additional tensions are obtained by definite integral

$$\bar{h}_{\tau 1} = \frac{\frac{EA}{l_1}(\Delta\bar{x}_1 - \Delta\bar{x}_2)}{1 - \left(\frac{\lambda_1}{\bar{\omega}_1}\right)^2(1 - \tan(\bar{\omega}_1/2)/(\bar{\omega}_1/2))} \tag{11a}$$

$$\bar{h}_{\tau 2} = \frac{\frac{EA}{l_2}\Delta\bar{x}_2}{1-(\frac{\lambda_2}{\bar{\omega}_2})^2(1-\tan(\bar{\omega}_2/2)/(\bar{\omega}_2/2))} \tag{11b}$$

and

$$\lambda_1^2 = \frac{EAl_1}{HL_{e1}}(\frac{ql_1}{H})^2 \approx \frac{EA}{H}(\frac{ql_1}{H})^2 \quad \lambda_2^2 \approx \frac{EA}{H}(\frac{ql_2}{H})^2 \tag{12}$$

The dynamic stiffness, K_h, is the ratio of the applied force to the corresponding displacement. From (11) and (9), the dynamic stiffness function would then be given by the expression

$$K_{dyn} = \lim_{\Delta x_1 \to 0}\frac{\Delta F}{\Delta x_1} = \frac{a_1[(a_2+\frac{1}{a}(T_{r1}+T_{l2}+\frac{W}{2}-\frac{J\omega^2}{a})]}{a_1+a_2+\frac{1}{a}(T_{r1}+T_{l2}+\frac{W}{2}-\frac{J\omega^2}{a})} \tag{13}$$

The remaining quantities are defined as

$$a_1 = \frac{EA}{l_1(1-\frac{\lambda_1^2}{\bar{\omega}_1^2}(1-\frac{\tan(\bar{\omega}_1/2)}{\bar{\omega}_1/2}))};$$
$$a_2 = \frac{EA}{l_2-l_2\frac{\lambda_2^2}{\bar{\omega}_2^2}(1-\frac{\tan(\bar{\omega}_2/2)}{\bar{\omega}_2/2})} \tag{14}$$

(13) is the most important equation in this paper. It is of significant practical value and teaches an important, fundamental way of approaching and diagnosing engineering problems. Upon carrying out the limiting transition $\omega \to 0$, (13) reduces to

$$K_s = \lim_{\Delta x_1 \to 0}\frac{\Delta F}{\Delta x_1} = \frac{\frac{EA}{l_1(1+\frac{1}{12}\lambda_1^2)}[(\frac{EA}{l_2(1+\frac{1}{12}\lambda_2^2)}+\frac{1}{a}(T_{r1}+T_{l2}+\frac{W}{2})]}{\frac{EA}{l_1(1+\frac{1}{12}\lambda_1^2)}+\frac{EA}{l_2(1+\frac{1}{12}\lambda_2^2)}+\frac{1}{a}(T_{r1}+T_{l2}+\frac{W}{2})} \tag{15}$$

K_s is equivalent static stiffness of two-span conductors.

A typical 500kV transmission line section, which consists of two-span quad bundle conductors, suspension clamp, and an insulator string, is selected to obtain the dynamic stiffness. The span lengths of first and second spans are the same as 200m. Each sub-conductor of quad bundle conductors is LGJ-400/50, mass per unit length 1.511kg/m, Young's modulus E is 7.0×10^4MPa, and the dimension of the conductor is 27.63×10^{-3}m. The suspension clamp is LX-4245, and its total mass is 89kg. The spacer is JZF-400, and its mass is 7.5kg. A suspension insulator consists of 28 ball-and-socket porcelain insulators of model XP-16 with self-weight 6.0kg, the length of suspension insulator string is 6.47m, and its Young's modulus is set to 200GPa. The tension stress at its lowest point in the conductor under self-weight is 30.3Mpa ($\lambda_1 = \pi$). It is noted that for quad bundle conductors the mass per unit length m in (13) is four times larger than a single conductor.

The variation of dynamic stiffness, K_d, with respect to the dimensionless frequency, $\bar{\omega}_1/\pi$, is shown in Fig.3 for the cable having two equal spans. The dynamic stiffness in each figure is normalized with respect to the corresponding static stiffness value. The static stiffness value calculated by (15) is constant, and the dynamic stiffness, which is calculated according to (13), is variable with frequency. In Fig.3(a) the peak corresponds to the frequency of first symmetrical mode, and in Fig.3(b) the first peak corresponds to the frequency of second symmetrical mode. The first peak in Fig.3(b) is much larger than the peak in Fig.3(a), it is shown from (13) that the effect of second symmetrical mode on the tension is much larger than the first symmetrical mode. This phenomenon of two-span conductors is different from single span.

In Fig3, the red line corresponds to a dynamic stiffness of quad bundle conductors, and the blank line corresponds to a dynamic stiffness of single conductor. It is shown from Fig.3 that the frequency of single-conductor is very close to that of quad bundle conductors when the geometrical and material parameters of single conductor and bundle conductors are the same. This conclusion provides a way to simplify the calculation of bundle conductors. In order to verify the validity of (13), the corresponding finite element model is established in ABAQUS. The frequencies of first two symmetrical modes of single conductor and bundle conductors obtained by ABAQUS are respectively 0.3536Hz, 0.4741Hz, 0.3515Hz and 0.4727Hz, respectively. The corresponding dimensionless frequencies are respectively 1.000, 1.340, 0.9937, and 1.336. The results obtained by ABAQUS showed that the frequency of single-conductor is very close to that of quad bundle conductors. The natural frequencies of single-conductor and quad bundle conductors, which are identified from Fig.3, are close to those obtained by the ABAQUS.

In order to simplify the theoretical formula for two-span conductors, the effect of insulator strings mass on the dynamic stiffness is studied. The black line corresponds to the dynamic stiffness of two equal spans considering insulator string mass, and the red line corresponds to the dynamic stiffness of two equal spans under the assumption of ignoring insulator string mass. The comparison of the frequency identified from Fig.4 is shown that the effect of insulator string mass on the frequency of two-span conductors is very small. Therefore, the J in (13) can be ignored when this (13) is used to calculate the frequency of two-span conductors.

Next, applying some examples, which have the same material parameters, insulator string length, and horizontal tension under self-weight as the previous examples, we will investigate the effects of the span ratio l_1/l_2 on dimensionless natural frequencies. In particular, first assuming that a constant first span length of l_1 is 200m, the second span length of l_2 is changed. Fig.5(a) shows the variation of the dynamic stiffness of the two-span transmission lines with different span ratios when first span length of l_1 is larger than the second span length of l_2. In particular, these peaks of dynamic stiffness represent the dimensionless natural frequencies of first symmetrical mode. It is seen that the dimensionless frequencies of corresponding first five peaks are greater than 1. It is possible to note that the dimensionless natural frequency of first symmetrical mode is decreasing as the ratio of l_1/l_2decreases. When the ratio of is reduced to 1 the dimensionless natural

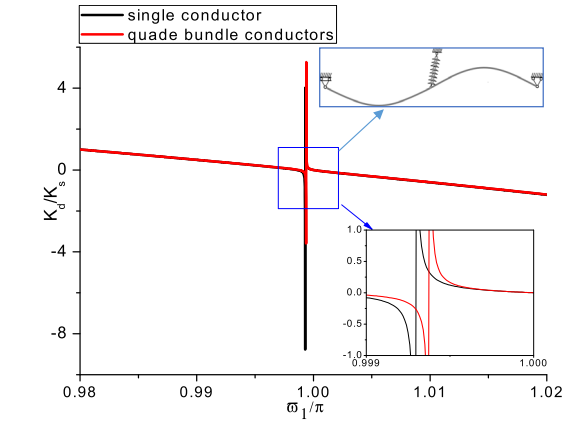

(a) Frequency of first symmetrical mode

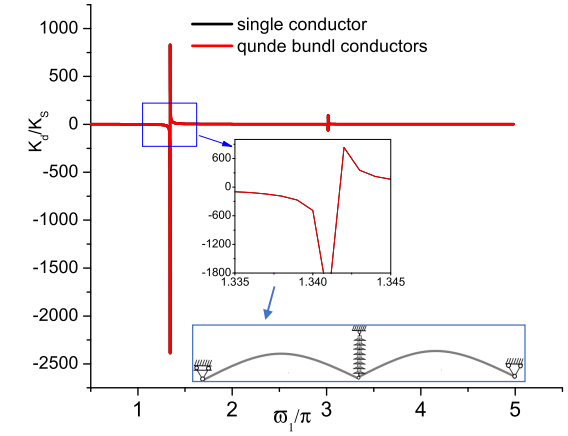

(b) Frequency of second symmetrical mode

FIGURE 3. Effect of sub-conductor number on the dynamic stiffness.

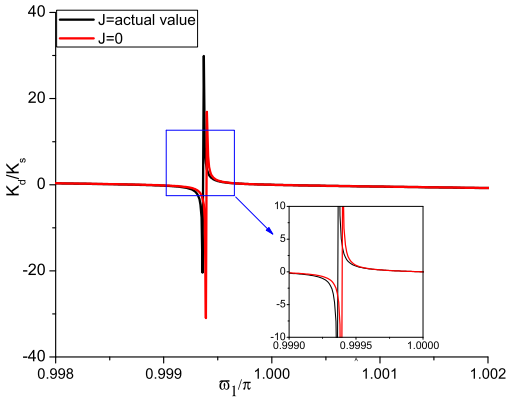

(a) Frequency of first symmetrical mode

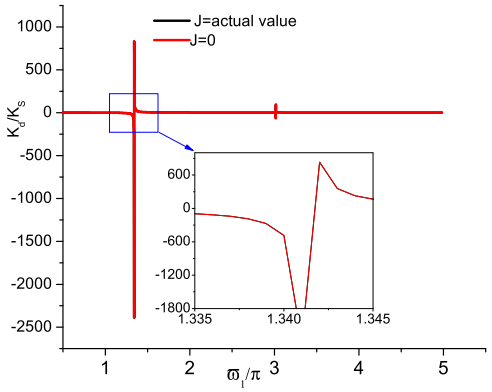

(b) Frequency of second symmetrical mode

FIGURE 4. Effect of insulator string mass on the dynamic stiffness.

frequency of first symmetrical mode is close to 1 by Combining the results of Fig.2. Fig.5(b) shows the variation of the dynamic stiffness of the two-span transmission lines with different span ratios when the first span length of l_1 is less than the second span length of l_2. It is seen that the dimensionless natural frequency of first symmetrical mode is increasing as the ratio of l_1/l_2 is increases, and when the ratio of l_1/l_2 increases to 1 the dimensionless natural frequency is closed to 1. Because of the first-span conductor is relatively long, so the first symmetrical mode is dominated by the vibration of the first-span conductor. With the reduction of the pitch of the second-span conductor, the restraint of the second-span conductor on the first-span conductor increases, resulting in an increase in the vibration frequency of the first-span conductor.

The dynamic stiffness formula can also be used to evaluate the natural frequencies of corresponding symmetrical modes by the peak of a dynamic stiffness. When first span length is a constant of 200m, the variation of the natural frequencies with span length ratio of l_1/l_2 is obtained from the peak of the dynamic stiffness of two spans at $\lambda_1/\pi = 1$ and $a = 6.47$ as shown in Fig.6. It is seen that the dimensionless natural frequencies of first two symmetrical modes are increasing as the ratio of span lengths increases. A scatter plot in Fig.6 presents the natural frequency obtained by ABAQUS. It is indicated that the natural frequency obtained by the dynamic stiffness is consistent with the ABAQUS result. On the other hand, the comparison between two methods shows that the dynamic stiffness formula is reasonable. The modes in Fig.6 shown that the ratio of span lengths has a significant effect on the mode shape of two spans. For the mode of two spans with 200m-50m, the modal displacement of the second span is close to 0. The first two symmetrical modes show that the modal displacement of a span having longer span length dominates when the length of a span in two span transmission lines is much greater than the length of another span.

In order to obtain a full understanding of the dynamic stiffness, the variation of the dynamic stiffness with dimensionless natural frequency is carried out on two-span conductors of 200m-250m, see Fig.7. Fig.7(a) shows the variation of the dynamic stiffness with dimensionless natural frequency for different insulator string lengths when the span lengths are 200m-250m and the λ_1/π is 1. For $\lambda_1/\pi = 1$, the insulator string length strongly influences the peak of dynamic stiffness. The dimensionless natural frequency of first symmetrical mode decreases from 0.90 to 0.89, when the insulator string length increases from 1m to 50m. It is shown that the insulator string length has few effect on dimensionless natural frequency when $\lambda_1/\pi = 1$.

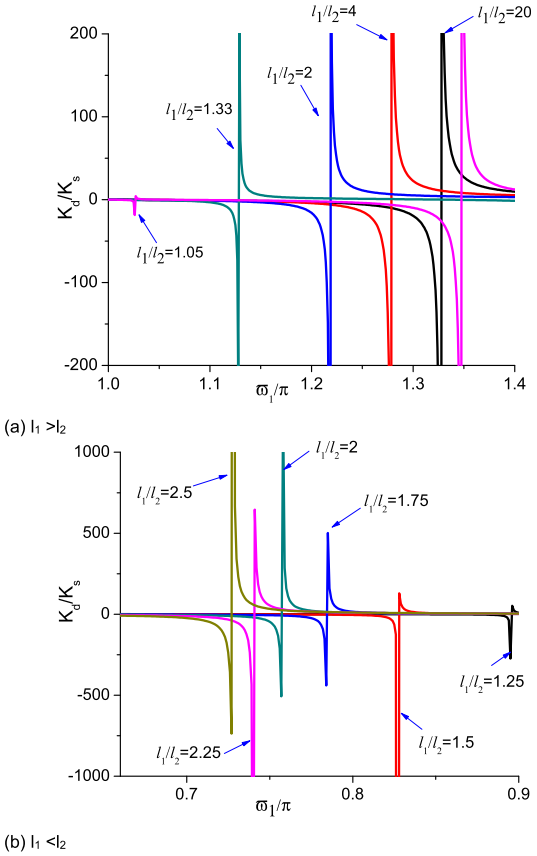

FIGURE 5. Effect of span lengths ratio on the dynamic stiffness ($\lambda_1/\pi = 1$; a = 6.47).

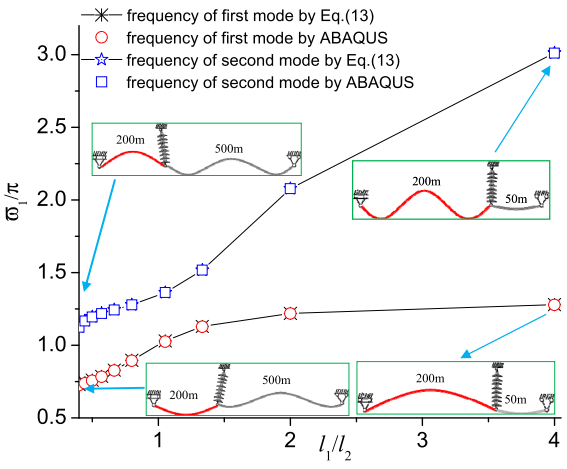

FIGURE 6. Variation of natural frequencies with span length ratio of l_1/l_2.

Fig.7(b) reports the variation of the dynamic stiffness with dimensionless natural frequency for different insulator strings when the span lengths are 200m-250m and the λ_1/π is 7. The calculated results also show that the insulator length has a remarkable effect on dynamic stiffness. In particular, the minimum peak occurs at the dimensionless natural frequency close to 1. This conclusion is in accord with what we discussed in Fig.6. As the insulator string length increases from 1m to 20m, the dimensionless natural frequency decreases from 1.15 to 0.92. For the two span transmission liens with $\lambda_1/\pi = 1$, the insulator string length has a remarkable effect

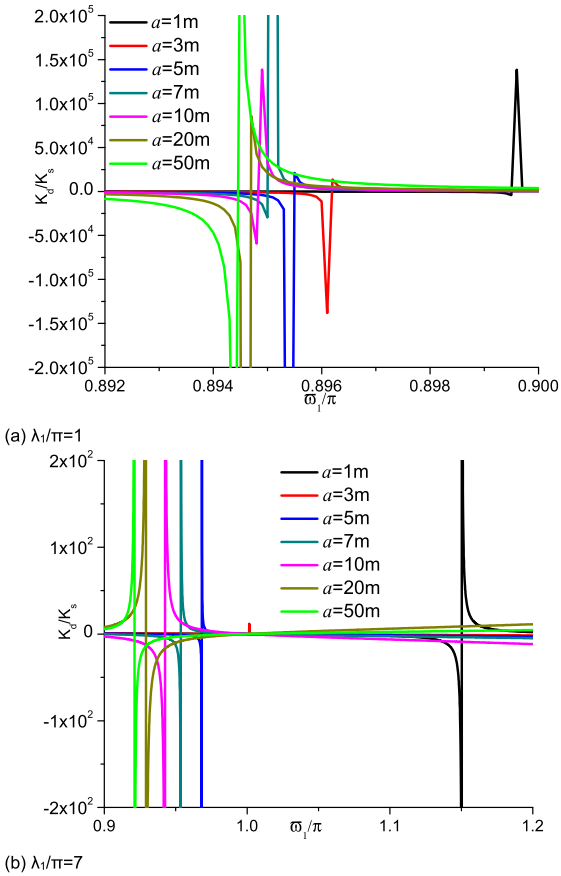

FIGURE 7. Effect of insulator string length on the dynamic stiffness (200m-250m).

on the dimensionless natural frequency by comparison with Fig.7(a). Fig.7(a) and (b) highlights a similar trend in the dimensionless natural frequency as a function of the insulator string length.

The solid lines in Fig.8 show that the variation of dimensionless natural frequencies with insulator string length obtained through dynamic stiffness peak in Fig.7. The calculated results show approximate constant natural frequency for $\lambda_1/\pi = 1$, whereas a dependency on insulator string length is found for $\lambda_1/\pi = 7$. In Fig.8 the scatter plots show that dimensionless natural frequencies are obtained by ABAQUS for different insulator string length. The theoretical results are generally consistent with those by ABAQUS. The maximum percent error between theory and ABAQUS results of 2.2% occurs at $\lambda_1/\pi = 7$ when insulator string length is 20m. The Fig.8 also shows that insulator string length has a few effect on symmetrical mode shape.

B. THEORETICAL FORMULA TO CALCULATE THE SYMMERTRICAL MODE

Substituting (13) into (11) and ignoring Δx_1, the i-th symmetrical modal shape can be written as

$$\phi_{1i}(x) = A_i \frac{\frac{1}{l_1}(1 - \tan(\frac{\bar{\omega}_1}{2})\sin(\bar{\omega}_1\frac{x}{l_1}) - \cos(\bar{\omega}_1\frac{x}{l_1}))}{1 - (\frac{\lambda_1}{\bar{\omega}_1})^2(1 - \tan(\bar{\omega}_1/2)/(\bar{\omega}_1/2))} \quad (16a)$$

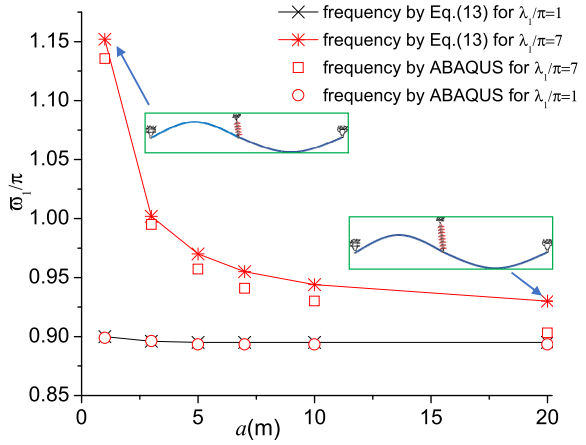

FIGURE 8. Variation of natural frequencies with insulator string of a (200m-250m).

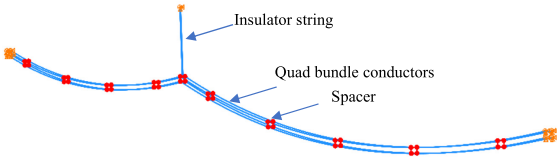

FIGURE 9. Finite element model of two-span conductors.

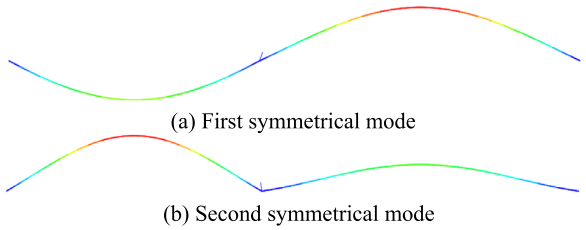

FIGURE 10. First two symmetrical modes obtained by ABAQUS.

$$\phi_{2i}(x) = A_i \frac{\frac{1}{l_2}(1-\tan(\frac{\bar{\omega}_2}{2})\sin(\bar{\omega}_2\frac{x}{l_2}) - \cos(\bar{\omega}_2\frac{x}{l_2}))}{1-(\frac{\lambda_2}{\bar{\omega}_2})^2(1-\tan(\bar{\omega}_2/2)/(\bar{\omega}_2/2))} \quad (16b)$$

where the A_i is determined by the normalization condition. When λ_1/π takes a large value, the (16) can be simplified as

$$\phi_{1i}(x) = B_i(1-\tan(\frac{\bar{\omega}_1}{2})\sin(\bar{\omega}_1\frac{x}{l_1}) - \cos(\bar{\omega}_1\frac{x}{l_1})) \quad (17a)$$

$$\phi_{2i}(x) = B_i(1-\tan(\frac{\bar{\omega}_2}{2})\sin(\bar{\omega}_2\frac{x}{l_2}) - \cos(\bar{\omega}_2\frac{x}{l_2})) \quad (17b)$$

where the B_i is determined by the normalization condition. In order to verify the validity of the new theoretical formulas, we use an example for comparison. We choose the geometrical parameters of two-span overhead transmission lines as follows: $l_1 = 200$m, $l_2 = 250$m, $a = 6.47$m. The material property settings are same with the first example for the insulators string and cable. The finite element model based on ABAQUS is established as follows:

Figure 10 shows the first two symmetrical modes of two-span conductors with $\lambda_1/\pi = 1$ is obtained by ABAQUS. The calculation modes show that the two adjacent spans influence each other.

In order to better understand the application range of (17) and (16), Fig.11 reports the comparison between the results

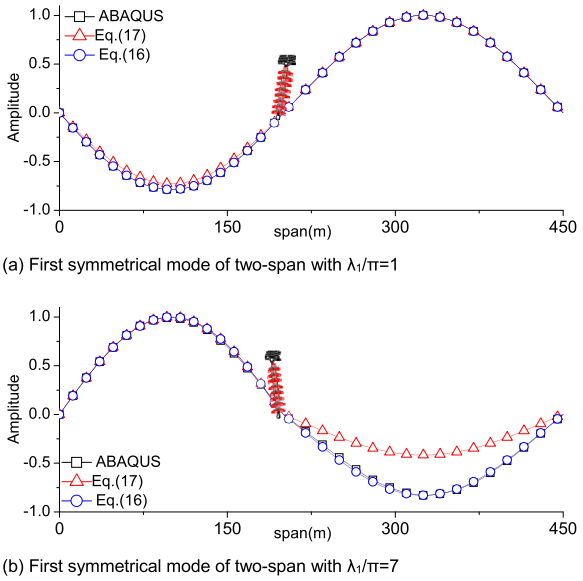

FIGURE 11. Comparison between the modes obtained by two methods.

of the two new theories and FEM method. It is interesting to observe that the results by the two methods agree well with that of ABAQUS when $\lambda_1/\pi = 1$, and only the result by (16) agrees with that of ABAQUS when $\lambda_1/\pi = 7$. It is shown that the simplified formula of (17) can be applied only to two-span conductors with a small sag, and the exact formula of (16) is also suitable for two- span conductors with a larger sag.

In order to understand the modal properties better, a factor β_i, which represents the ratio between the kinematic energy stored in a span conductor and the total kinematical energy of the two-span transmission lines having mono-frequent free linear vibration, is suggested. Based on the obtained closed-form solution of the mode of two-span transmission lines, the factor β_i for the j-th mode is defined as

$$\beta_{i1} = \frac{\int_0^{l_1} m\phi_{1i}^2(x)\frac{1}{l_1}\mathrm{d}x}{\int_0^{l_1} m\phi_{1i}^2(x)\frac{1}{l_1}\mathrm{d}x + \int_0^{l_2} m\phi_{1i}^2(x)\frac{1}{l_2}\mathrm{d}x} \quad (18a)$$

$$\beta_{i2} = \frac{\int_0^{l_2} m\phi_{2i}^2(x)\frac{1}{l_2}\mathrm{d}x}{\int_0^{l_1} m\phi_{2i}^2(x)\frac{1}{l_1}\mathrm{d}x + \int_0^{l_2} m\phi_{2i}^2(x)\frac{1}{l_2}\mathrm{d}x} \quad (18b)$$

where β_{i1} and β_{i2} reflect the contribution of the first and second span to the mode shape of the total system, respectively. In the following two examples, the effect of transmission line parameters on the localization factor is illustrated.

When the insulator lengths are, respectively, 1m and 7m in the two-span transmission lines, in which the span lengths are 200m and 250m, the variations of the localization factor of the first symmetrical mode with the λ_1/π are reported in Fig.12(a). It can be seen that when λ_1/π is in the range of 0∼2, the localization factor is decreases and when λ_1/π is in the range of 2∼10, the localization factor has a constant trend. The calculated results also show that when the two span lengths are 200m and 250m, the effect of the insulator string length on the localization factor is very small.

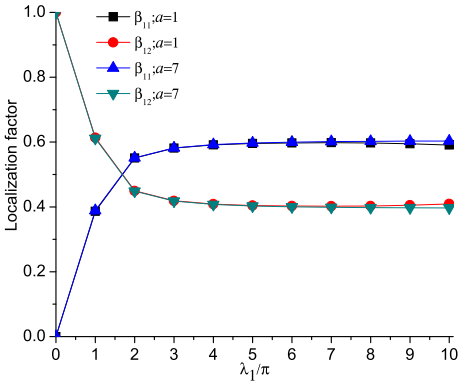

(a) Variation of the localization factor with the λ1

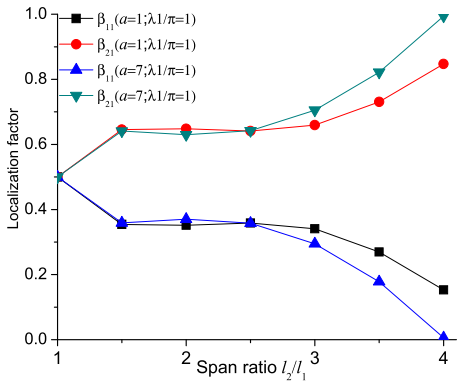

(b) Variation of the localization factor with the span ratio

FIGURE 12. Effect of the transmission line parameters on the localization factor.

When the insulator lengths are, respectively, 1m and 7m in the two-span transmission lines, in which the λ_1/π is equal to 1, the variation of the localization factor of the first symmetrical mode with the span ratio l_2/l_1 are in Fig.12(b). It is noted that when the value of l_2/l_1 is large, the span ratio and insulator string length have a significant effect on the localization factor.

III. DYNAMIC STIFFNESS FOR MULTI-SPAN CONDUCTOR

A. THEORETICAL FORMULA TO CALCULATE THE DYNAMIC STIFFNESS

Similarly, for multi-span transmission lines with arbitrary span number, the dynamical stiffness can be also obtained by referring to the calculation method of two-span conductors. Multi-span transmission lines with N spans are reported in Fig.13. All suspension points of $N-1$ insulator strings are located at the same level. The support A_1 is a smooth roller, and the support A_{N+1} is a hinge. Each span can be considered as a substructure, and local coordinate system, which is attached to each span at its left end, is established on the substructure. For example, the x_j-axis is taken along the chord of the j-th span, and the y_j-axis is taken along the vertical direction. w_j is the transverse displacement in the y_i direction.

If the left end A_1 of the transmission lines is subjected to an additional harmonically varying horizontal force

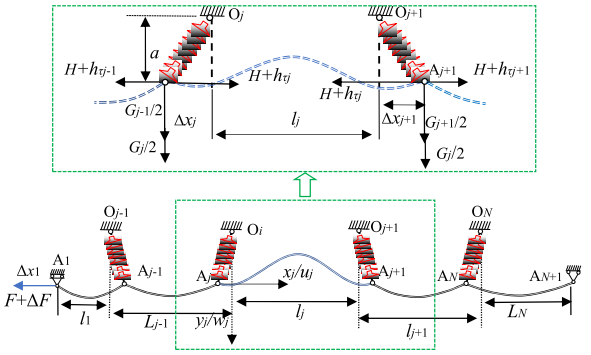

FIGURE 13. Multi-span transmission lines.

$\Delta F = \Delta\bar{F}e^{i\omega t}$, the dynamic configuration of the transmission lines is the dotted line as shown in Fig.13. Neglecting the conductor inertia component parallel to the chord, The vertical vibration of j-th span conductor with respect to its position of static equilibrium can be expressed by the partial differential equation [3]

$$H\frac{\partial^2 w_j}{\partial x^2} + h_{\tau j}\frac{\mathrm{d}^2 y_j}{\mathrm{d}x^2} = m\frac{\partial^2 w_j}{\partial t^2} + c\frac{\partial w_j}{\partial t} \tag{19}$$

where the $h_{\tau j}$ is the additional tension of j-th span conductor. y_j is the static equilibrium configuration of j-th span conductor with small sag, which is represented by (1). Solution to the partial differential can be obtained using the technique known as separation of variables. For j-th span conductor, we substitute (1) and (7) into the (19) to obtain

$$H\frac{\mathrm{d}^2\bar{w}_j}{\mathrm{d}x^2} + (m\omega^2 - i\omega c)\bar{w}_j = \frac{q\bar{h}_{\tau j}}{H} \tag{20}$$

The solution of (20), with the given boundary condition of $\bar{w}_j(0) = \bar{w}_j(l_j)$, is

$$\bar{w}_j(x) = (\frac{l_j}{\bar{\omega}_j H})^2 q h_{\tau j}(1 - \tan(\frac{\bar{\omega}_j}{2})\sin(\bar{\omega}_j\frac{x}{l_j}) - \cos(\bar{\omega}_j\frac{x}{l_j})) \tag{21}$$

were $\bar{\omega}_j^2 = (m\omega^2 - \omega c i)l_j^2/H$, $\bar{w}_j(x)$ is in-plane vertical displacement of j-th span conductor. Neglecting the inertia component parallel to the chord, substituting the (21) into the (6), the additional tension on j-th span conductor is obtained with the given boundary condition as

$$\bar{h}_{\tau j} = \frac{\frac{EA}{l_j}(\Delta\bar{x}_j - \Delta\bar{x}_{j+1})}{1 - (\frac{\lambda_j}{\bar{\omega}_j})^2(1 - \tan(\bar{\omega}_j/2)/(\bar{\omega}_j/2))} \tag{22}$$

where $\lambda_j^2 = \frac{EA}{H}(\frac{ql_j}{H})^2$, $\Delta\bar{x}_{N+1} = 0$ for N span transmission lines. N span transmission lines include $N-1$ insulator strings. For O_jA_j insulator string as shown in Fig.12, the sun of the moments about O of all the external forces is equal to $J\Delta\ddot{x}/a$. Considering the left end A_1 of multiple span transmission lines is subjected to a harmonically varying horizontal force, the following relation is obtained from the differential equation governing j-th insulator string rotation:

$$a(\bar{h}_{\tau j-1} - \bar{h}_{\tau j}) = (\frac{G_{j-1} + G_j}{2} + \frac{W}{2} - \frac{J\omega^2}{a})\Delta\bar{x}_j \tag{23}$$

were G_{j-1} is the self-weight of $(j-1)$-th span conductor, and G_j is the self-weight of j-th span conductor. $\Delta\bar{x}_j$ is the displacement amplitude of the low end of the i-th suspension insulator string. Then, based on (22)-(23) and the dynamic stiffness define $K_x = \lim_{\Delta x_1 \to 0} \frac{\Delta F}{\Delta x_1}$, the dynamic stiffness of multi-span transmission lines is given as (24), shown at the bottom of the page, were

$$K_i = \frac{EA}{l_i(1 - \frac{\lambda_i^2}{\bar{\omega}_i^2}(1 - \frac{\tan(\bar{\omega}_i/2)}{\bar{\omega}_i/2}))};$$
$$E_i = \frac{1}{a}(\frac{G_i + G_{i+1}}{2} + \frac{W}{2} - \frac{J\omega^2}{a}) \tag{25}$$

The dynamic stiffness is expressed also by recursive formula as

$$K_x = \frac{K_1(K_{2N} + E_1)}{K_1 + K_{2N} + E_1} \tag{26}$$

were

$$K_{iN} = \frac{K_i(K_{(i+1)N} + E_i)}{K_i + K_{(i+1)N} + E_i} \quad (1 < \mathrm{i} < \mathrm{N}) \tag{27a}$$
$$K_{iN} = K_N \quad (\mathrm{i} = \mathrm{N}) \tag{27b}$$

In order to verify the validity of the dynamic stiffness of multi-span transmission lines, we use some examples for comparison. The material parameters for the following two examples are same as for the first example in this paper. For the transmission lines with three spans of 100m-140m-180m that the insulator string length is 6.47m, and λ_1/π is 1 under self-weight, the variation of the dynamic stiffness with $\bar{\omega}_1/\pi$ is reported in Fig.14(a). The dimensionless natural frequencies can be identified by these peaks of the dynamic stiffness. It is shown in Fig.14(a) that the natural frequencies identified by the dynamic stiffness are close to those obtained by ABAQUS method. The Fig.14(a) also shows that the values of the second, third and fourth peaks are significantly greater than those of other peaks. It is indicated that the energy is easily transferred to an adjacent structure when the resonance of the transmission lines includes the modes that correspond to the natural frequencies of the second, third and fourth peaks.

For the transmission lines with five spans of 100m-140m-180m-220m-260m having the insulator string length of 6.47m and λ_1/π of 1, the variation of the dynamic stiffness with respect to the dimensionless frequency of $\bar{\omega}_1/\pi$ is reported in Fig.14(b). A good agreement between the dimensionless natural frequencies by the two methods in Fig.14(b) further provides proof of the correctness of the dynamic stiffness. Similar to three spans, the Fig.14(b) shows the maximum peak value of the fourth peak, and the energy is easily transferred to an adjacent structure when the resonance of the five-span transmission lines includes the fourth symmetrical mode.

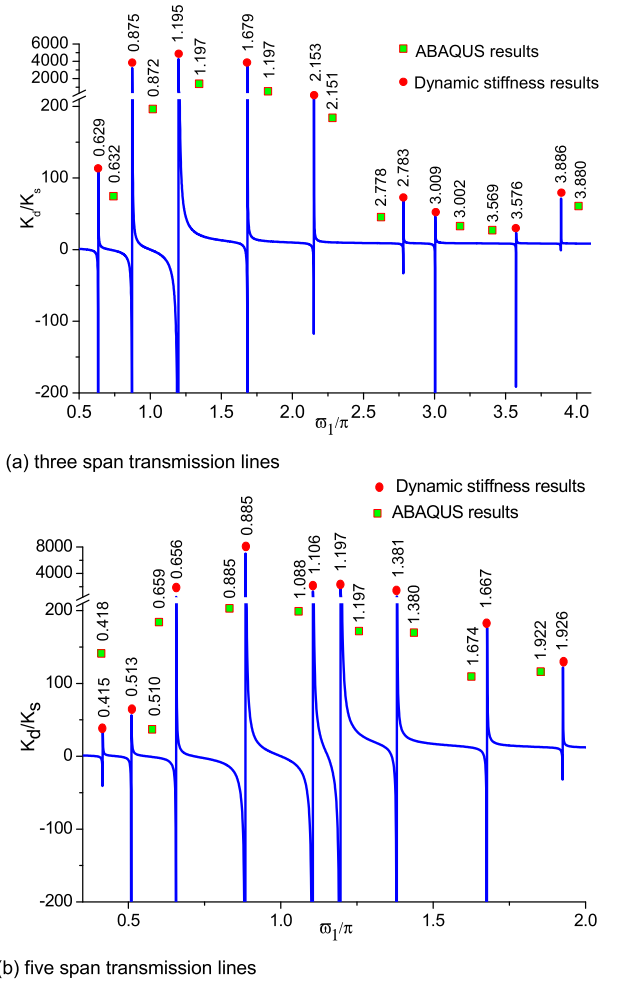

(a) three span transmission lines

(b) five span transmission lines

FIGURE 14. Dynamic stiffness of transmission lines with different span numbers.

$$\begin{vmatrix} K_x - K_1 & K_1 & 0 & 0 & 0 & 0 & \cdots \\ -K_1 & K_1 + K_2 + E_1 & -K_2 & 0 & 0 & 0 & \cdots \\ 0 & \ddots & \ddots & \ddots & \ddots & \ddots & \cdots \\ \vdots & 0 & -K_i & K_i + K_{i+1} + E_i & -K_{i+1} & 0 & \cdots \\ 0 & \cdots & 0 & \ddots & \ddots & \ddots & \cdots \\ \vdots & \vdots & \vdots & 0 & -K_{N-2} & K_{N-2} + K_{N-1} + E_{N-2} & -K_{N-1} \\ 0 & 0 & \cdots & \cdots & \cdots & -K_{N-1} & K_{N-1} + K_N + E_{N-1} \end{vmatrix} = 0 \tag{24}$$

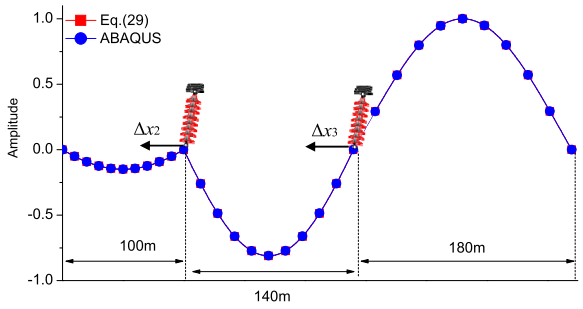

FIGURE 15. Comparison between the three-span modes obtained by two methods.

B. THEORETICAL FORMULA TO CALCULATE THE SYMMETRICAL MODE

For multi-span transmission lines having arbitrary span number, the modal function can be obtained by referring to the calculation method of two-span transmission lines. According to the (28), the symmetrical mode of N-span transmission lines can be obtained as follows:

$$\phi_i(x) = A_i \frac{\frac{\Delta x_i - \Delta x_{i+1}}{l_i}(1 - \tan(\frac{\bar{\omega}_i}{2})\sin(\bar{\omega}_i\frac{x}{l_i}) - \cos(\bar{\omega}_i\frac{x}{l_i}))}{1 - (\frac{\lambda_i}{\bar{\omega}_i})^2(1 - \tan(\bar{\omega}_i/2)/(\bar{\omega}_i/2))} \tag{28}$$

were $1 \le i \le N$, $\Delta x_1 = \Delta x_{N+1} = 0$. In (28) $\Delta x_2, \Delta x_3 \ldots$ are unknown quantities and can be obtained as the equation (29), shown at the bottom of the page.

In order to verify to the validity of Eq.(29), according to the preceding of three-span transmission lines with 100m-140m-180m having the insulator string length of 6.47m and λ_1/π of 1, the dimensionless natural frequency corresponding first symmetrical mode is obtained from Fig.14(a) and is equal to 0.629. Substituting 0.629 into (29), we obtain $\Delta x_3/\Delta x_2$ of 5.8. According to corresponding geometrical and material parameters of this three-span transmission lines, Δx_2 and Δx_3 in first symmetrical mode are obtained from ABAQUS and are equal to -0.0132m and -0.0777m, respectively. The $\Delta x_3/\Delta x_2$ obtained by ABAQUS is 5.9 and is close to that with (29). Substituting the parameters of three-span transmission lines and $\Delta x_3/\Delta x_2$into (29), the first symmetrical mode of the three-span conductors is obtained as shown in Fig.15. It is indicated that the two first symmetrical modes obtained by two methods are in good agreement.

IV. CONCLUSION

In this paper, a theoretical method for the calculation of equivalent dynamic stiffness is presented. Unlike previous dynamic stiffness of a single span, the effect of the adjacent span and swing of insulator string are considered. The parametric study reveals that the previously ignored factor, as the insulator string length, is indeed very important for the dynamic stiffness. The sizes of the peaks that correspond to different modes are not the same.

The natural frequencies are identified based on the peak-to-peak of the dynamic stiffness curve with varying external exciting frequency, and corresponding modes are obtained. The validity and accuracy of the proposed frequencies and the associated modes are verified by using finite element method. It is shown that the method is accuracy, and more convenient than the finite element method. At the same time, a parametric study is performed to examine the sensitivity of the natural frequencies and associated modes to the span ratio, insulator length, Irvine parameters, and span number. In particular, the mode localization is discussed.

In this paper the main contribution is a closed-form expression for the dynamic stiffness of arbitrary multi-span transmission lines. The dynamic stiffness and natural frequencies obtained by the dynamic stiffness can be used to guide the design of overhead transmission lines so as to avoid the coupling between towers and liens or coupling between different spans, which may cause severe damage of transmission lines.

$$\begin{Bmatrix} K_1+K_2+E_1 & -K_2 & 0 & 0 & 0 & 0 & \cdots \\ -K_2 & K_2+K_3+E_2 & -K_3 & 0 & 0 & 0 & \cdots \\ 0 & \ddots & \ddots & \ddots & 0 & 0 & \cdots \\ \vdots & 0 & -K_i & K_i+K_{i+1}+E_i & -K_{i+1} & 0 & \cdots \\ 0 & & 0 & \ddots & \ddots & \ddots & \cdots \\ \vdots & \vdots & \vdots & 0 & -K_{N-2} & K_{N-2}+K_{N-1}+E_{N-2} & -K_{N-1} \\ 0 & 0 & \cdots & \cdots & \cdots & -K_{N-1} & K_{N-1}+K_N+E_{N-1} \end{Bmatrix} \times \begin{Bmatrix} \Delta x_2 \\ \Delta x_3 \\ \vdots \\ \\ \\ \Delta x_N \end{Bmatrix} = 0 \tag{29}$$

ACKNOWLEDGMENT

The authors declare that there is no conflict of interests regarding the publication of this article.

REFERENCES

[1] M. Kermani, M. Farzaneh, and L. E. Kollar, "The effects of wind induced conductor motion on accreted atmospheric ice," *IEEE Trans. Power Del.*, vol. 28, no. 2, pp. 540–548, Apr. 2013.

[2] L. Chen, H. Zhang, C. Li, and H. Sun, "Modeling and simulating long-timescale cascading faults in power systems caused by line-galloping events," *Energies*, vol. 10, no. 9, p. 1301, Aug. 2017.

[3] State Grid. *State Grid was Put to the Test of a Wide Range of Freezing Rain and Snow Power Grid Will Test.* Accessed: Jan. 29, 2018. [Online]. Available: http://www.cma.gov.cn/2011xwzx/2011xmtjj/201801/t20180129_461252.html

[4] H. M. Irvine and T. K. Caughey, "The linear theory of free vibrations of a suspended cable," *Proc. Roy. Soc. London, A, Math. Phys. Sci.*, vol. 341, pp. 299–315, Dec. 1974.

[5] H. M. Irvine, "Free vibrations of inclined cables," *J. Struct. Division*, vol. 104, no. 2, pp. 343–347, Feb. 1978.

[6] H. Yamaguchi and M. Ito, "Linear theory of free vibrations of an inclined cable in three dimensions," *Proc. Jpn. Soc. Civil Eng.*, vol. 1979, no. 286, pp. 29–36, 1979.

[7] M. S. Triantafyllou, "The dynamics of taut inclined cables," *Quart. J. Mech. Appl. Math.*, vol. 37, no. 3, pp. 421–440, 1984.

[8] M. S. Triantafyllou and L. Grinfogel, "Natural frequencies and modes of inclined cables," *J. Struct. Eng.*, vol. 112, no. 1, pp. 139–148, Jan. 1986.

[9] Q. Wu, K. Takahashi, and S. Nakamura, "Formulae for frequencies and modes of in-plane vibrations of small-sag inclined cables," *J. Sound Vib.*, vol. 279, nos. 3–5, pp. 1155–1169, Jan. 2005.

[10] X. Zhou, S. Yan, and F. Chu, "In-plane free vibrations of an inclined taut cable," *J. Vib. Acoust.*, vol. 133, no. 3, Jun. 2011, Art. no. 031001.

[11] A. S. Veletsos and G. R. Darbre, "Dynamic stiffness of parabolic cables," *Earthq. Eng. Struct. Dyn.*, vol. 11, no. 3, pp. 367–401, May 1983.

[12] J. Kim and S. P. Chang, "Dynamic stiffness matrix of an inclined cable," *Eng. Struct.*, vol. 23, no. 12, pp. 1614–1621, Dec. 2001.

[13] H. Yuan, E. Courteille, M. Gouttefarde, and P.-E. Hervé, "Vibration analysis of cable-driven parallel robots based on the dynamic stiffness matrix method," *J. Sound Vib.*, vol. 394, pp. 527–544, Apr. 2017.

[14] L. Jun, B. Yuchen, and H. Peng, "A dynamic stiffness method for analysis of thermal effect on vibration and buckling of a laminated composite beam," *Arch. Appl. Mech.*, vol. 87, no. 8, pp. 1295–1315, Aug. 2017.

[15] W. Dai, C. Shi, Y. Tan, and F. Rojas, "A numerical solution and evaluation of dynamic stiffness of pile groups and comparison to experimental results," *Eng. Struct.*, vol. 151, pp. 253–260, Nov. 2017.

[16] L. Kari, "Dynamic stiffness of chemically and physically ageing rubber vibration isolators in the audible frequency range: Part 2—Waveguide solution," *Continuum Mech. Thermodyn.*, vol. 29, no. 5, pp. 1047–1059, Sep. 2017.

[17] B.-H. Li, H.-S. Gao, H.-B. Zhai, Y.-S. Liu, and Z.-F. Yue, "Free vibration analysis of multi-span pipe conveying fluid with dynamic stiffness method," *Nucl. Eng. Des.*, vol. 241, no. 3, pp. 666–671, Mar. 2011.

[18] G. Rega, W. Lacarbonara, A. H. Nayfeh, and C. M. Chin, "Multiple resonances in suspended cables: Direct versus reduced-order models," *Int. J. Non-Linear Mech.*, vol. 34, no. 5, pp. 901–924, Sep. 1999.

[19] G. Rega, "Nonlinear vibrations of suspended cables—Part I: Modeling and analysis," *Appl. Mech. Rev.*, vol. 57, no. 6, pp. 443–478, Nov. 2004.

[20] A. H. Nayfeh, H. N. Arafat, C.-M. Chin, and W. Lacarbonara, "Multimode interactions in suspended cables," *J. Vib. Control*, vol. 8, no. 3, pp. 337–387, Mar. 2002.

[21] W. Lacarbonara, G. Rega, and A. H. Nayfeh, "Resonant non-linear normal modes. Part I: Analytical treatment for structural one-dimensional systems," *Int. J. Non-Linear Mech.*, vol. 38, no. 6, pp. 851–872, Sep. 2003.

[22] N. Srinil, G. Rega, and S. Chucheepsakul, "Two-to-one resonant multimodal dynamics of horizontal/inclined cables. Part I: Theoretical formulation and model validation," *Nonlinear Dyn.*, vol. 48, no. 3, pp. 231–252, Feb. 2007.

[23] A. Abe, "Validity and accuracy of solutions for nonlinear vibration analyses of suspended cables with one-to-one internal resonance," *Nonlinear Anal., Real World Appl.*, vol. 11, no. 4, pp. 2594–2602, Aug. 2010.

[24] Y. Zhao and L. Wang, "On the symmetric modal interaction of the suspended cable: Three-to-one internal resonance," *J. Sound Vib.*, vol. 294, nos. 4–5, pp. 1073–1093, Jul. 2006.

[25] L. Wang, Y. Zhao, and G. Rega, "Multimode dynamics and out-of-plane drift in suspended cable using the kinematically condensed model," *J. Vib. Acoust.*, vol. 131, no. 6, Dec. 2009, Art. no. 061008.

[26] A. Luongo and G. Piccardo, "Non-linear galloping of sagged cables in 1:2 internal resonance," *J. Sound Vib.*, vol. 214, no. 5, pp. 915–940, Jul. 1998.

[27] A. Luongo, D. Zulli, and G. Piccardo, "Analytical and numerical approaches to nonlinear galloping of internally resonant suspended cables," *J. Sound Vib.*, vol. 315, no. 3, pp. 375–393, Aug. 2008.

[28] A. Luongo and G. Piccardo, "A continuous approach to the aeroelastic stability of suspended cables in 1:2 internal resonance," *J. Vib. Control*, vol. 14, nos. 1–2, pp. 135–157, Jan. 2008.

[29] A. Luongo, D. Zulli, and G. Piccardo, "On the effect of twist angle on nonlinear galloping of suspended cables," *Comput. Struct.*, vol. 87, nos. 15–16, pp. 1003–1014, Aug. 2009.

[30] X.-H. Liu, B. Yan, H.-Y. Zhang, and S. Zhou, "Nonlinear numerical simulation method for galloping of iced conductor," *Appl. Math. Mech.*, vol. 30, no. 4, pp. 489–501, Apr. 2009.

[31] L. Fu-Hao, Z. Qi-Chang, and T. Ying, "Analysis of high codimensional bifurcation and chaos for the quad bundle conductor's galloping," *Chin. Phys. Lett.*, vol. 27, no. 4, Apr. 2010, Art. no. 044702.

[32] Z. Yan, Z. Yan, Z. Li, and T. Tan, "Nonlinear galloping of internally resonant iced transmission lines considering eccentricity," *J. Sound Vib.*, vol. 331, no. 15, pp. 3599–3616, Jul. 2012.

[33] X. Liu and B. Huo, "Nonlinear vibration and multimodal interaction analysis of transmission line with thin ice accretions," *Int. J. Appl. Mech.*, vol. 7, no. 1, Feb. 2015, Art. no. 1550007.

[34] H. Guo, B. Liu, Y. Yu, S. Cao, and Y. Chen, "Galloping suppression of a suspended cable with wind loading by a nonlinear energy sink," *Arch. Appl. Mech.*, vol. 87, no. 6, pp. 1007–1018, Jun. 2017.

[35] W. Lou, L. Yang, M. F. Huang, and X. Yang, "Two-parameter bifurcation and stability analysis for nonlinear galloping of iced transmission lines," *J. Eng. Mech.*, vol. 140, no. 11, Nov. 2014, Art. no. 04014081.

[36] S. Ghabraei, H. Moradi, and G. Vossoughi, "Finite time-Lyapunov based approach for robust adaptive control of wind-induced oscillations in power transmission lines," *J. Sound Vib.*, vol. 371, pp. 19–34, Jun. 2016.

[37] D. Zhang, Z. He, Z. Huang, and W. Jiang, "Isogeometric collocation method for the galloping of an iced conductor," *J. Eng. Mech.*, vol. 143, no. 5, May 2017, Art. no. 04017009.

[38] C. H. Nguyen and J. H. G. Macdonald, "Galloping analysis of a stay cable with an attached viscous damper considering complex modes," *J. Eng. Mech.*, vol. 144, no. 2, Feb. 2018, Art. no. 04017175.

[39] S. W. Rienstra, "Nonlinear free vibrations of coupled spans of overhead transmission lines," *J. Eng. Math.*, vol. 53, nos. 3–4, pp. 337–348, Dec. 2005.

[40] P. Yu, Y. M. Desai, A. H. Shah, and N. Popplewell, "3-degree-of-freedom model for galloping. 2. Somutions," *J. Eng. Mech.*, vol. 119, no. 12, pp. 2426–2448, 1993.

[41] Y. M. Desai, Y. A. H. Shah, and N. Popplewell, "Perturbation-based finite element analyses of transmission line galloping," *J. Sound Vib.*, vol. 191, no. 4, pp. 469–489, Apr. 1996.

[42] L. Guo and L. Li, "Effect of temperature on galloping of iced conductor," *Adv. Struct. Eng.*, vol. 21, no. 1, pp. 3–13, 2018.

[43] X. Wang and W. J. Lou, "Numerical approach to the gallop of iced conductor," *Eng. Mech.*, vol. 27, no. 1, pp. 290–293, 2010.

[44] X. Wang and W. J. Lou, "Numerical approach to galloping of conductor," in *Proc. 7th Asia–Pacific Conf. Wind Eng.*, Taipei, Taiwan, Nov. 2009.

[45] X. Xie, X. Hu, J. Peng, and Z. Wang, "Refined modeling and free vibration of two-span suspended transmission lines," *Acta Mechanica*, vol. 228, no. 2, pp. 673–681, Feb. 2017.

[46] Z. Yi, Z. Wang, Y. Zhou, and I. Stanciulescu, "Modeling and vibratory characteristics of a mass-carrying cable system with multiple pulley supports in span range," *Appl. Math. Model.*, vol. 49, pp. 59–68, Sep. 2017.